The Case for Phytoplankton Blooms Under Antarctic Sea Ice

C. Horvat[1], S. Seabrook[2,3], A. Cristi[2,4], L. Matthes[5], K. Bisson[6]

[1]Institute at Brown for Environment and Society, Brown University, Providence, RI, USA
[2]National Institute of Water and Atmospheric Research, Wellington, NZ
[3]School of the Environment, University of Auckland, Auckland, NZ
[4]Department of Marine Sciences, University of Otago, Dunedin, NZ
[5]Centre for Earth Observation Science, University of Manitoba, Winnipeg, MB, CA
[6]Department of Botany and Plant Pathology, Oregon State University, Corvallis, OR, USA

Key Points:

- We use ICESat-2 and CMIP6 data to make the first assessment of under-sea-ice blooms in the Southern Hemisphere.
- Light, ice, and ocean conditions permit widespread blooming before the seasonal retreat of Southern Ocean sea ice.
- We identify areas where direct sampling can be employed to assess the validity of these study results.

Corresponding author: Chris Horvat, `horvat@brown.edu`

Abstract

Being highly reflective and absorptive, sea ice was often assumed to prohibit upper ocean photosynthesis - yet observations in the modern Arctic reveal widespread under-ice blooms, driven by a transition to thinner, more mobile first-year sea ice - superficially similar to that found in the Southern Ocean. No studies have quantified the potential for under-sea-ice blooms at the Southern Ocean scale. Here we examine Southern Ocean light, sea ice, and ocean conditions, using 11 climate model contributions to CMIP6 and the ICESat-2 laser altimeter. We find large areas, 4 million square kilometers or more, of the sea-ice-covered Southern Ocean are hospitable to upper ocean photosynthesis. A stronger focus on these regions through field and remote sensing studies is necessary to assess the possible impact of under-ice productivity on Southern Hemisphere carbon and nutrient cycling.

1 Introduction

The observation of under-ice phytoplankton blooms in the Arctic Ocean (Arrigo et al., 2012) spurred intense interest in the ecological communities living in the ocean under Arctic sea ice and their fate under climate change (Ardyna et al., 2020, and references within). Less attention has been to conditions under Antarctic sea ice. As the Arctic sea ice cover continues to trend toward thinner, younger ice, it becomes more physically similar to Antarctic sea ice, which is seasonal, with an annual sea ice maximum covering an area approximately 6 times larger than the annual minimum. Because snow is present on Antarctic sea ice year-round, and a large fraction of Antarctic sea ice forms through surface flooding, its albedo is typically higher than Arctic sea ice (Brandt et al., 2005; Arndt et al., 2017). Yet the geography of the Antarctic continent positions Antarctic sea ice more equatorward than Arctic sea ice, resulting in an approximately 50% higher solar radiation input compared to Arctic sea ice over the course of the year (Gelaro et al., 2017). Sea ice in the Southern Ocean is also mobile, which can promote the opening of small areas of open water, leads, through which light can reach the upper ocean. Sunlight entering the ocean through small areas of open water can initiate a phytoplankton bloom even where sea ice is thick and snow-covered (Assmy et al., 2017; Lowry et al., 2018).

The Southern Ocean is a highly productive place (Deppeler & Davidson, 2017, and references within). Phytoplankton communities in the Southern Ocean mainly consist

of diatoms and flagellates (Davidson et al., 2010; Arrigo et al., 2017), with community composition and phytoplankton size-structure strongly influenced by sea ice (and therefore light) variability (Biggs et al., 2019; Montes-Hugo et al., 2008). In coastal Antarctic regions, blooms typically consist of diatoms or colonial haptophyte *Phaeocystis antarctica*. Observations in the ice-free Ross Sea have described a seasonal succession between the two; *P. antarctica* blooms in late spring under relatively deeper mixed layers (25-50 m), and diatom blooms in early summer under more stratified conditions (5-25 m) (Arrigo, 1999). As in the Arctic (Perrette et al., 2011), phytoplankton blooms are observed as soon as the sea ice edge retreats in the spring, flooding the mixed layer with light and leaving freshwater rich in iron, two of the main limiters of productivity (Martin et al., 1990; Comiso et al., 1993; van Oijen, 2004).

Crucial for the genesis of an under-ice bloom (UIB) is the formation of a stable surface mixed layer, which can be induced by melt water addition and/or increased solar heating of the surface layer (Lowry et al., 2018; Oziel et al., 2019). Observations from autonomous platforms and tagged seals, for example in the Ross Sea, show the initiation of ice melt forms a shallow (20 m), haline surface mixed layer, preceding the complete retreat of sea ice (Porter et al., 2019). This may present favorable conditions for UIBs because stable mixed layers entrain phytoplankton in the well-lit surface ocean. A recent pan-Southern-Ocean study of under-ice mixed layers from tagged seals and hydrographic data reveal mixed layers shallower than 50 m in November-December across ice-covered regions (Pellichero et al., 2017). Observations from under-ice biogeochemical ARGO floats suggest the initiation of primary production occurs before seasonal sea ice retreat, and even before the restratification of surface waters, challenging the notion that too-deep surface mixed layers in ice-covered regions of the Southern Ocean limit productivity (Arteaga et al., 2020; Hague & Vichi, 2021).

The numerous observations of UIBs, even under thick sea ice in the Arctic Ocean (Ardyna et al., 2020); the large solar fluxes to Southern Ocean sea ice; the characteristics of Southern Ocean sea ice and under-ice ocean properties; and the productivity of ice-free Southern Ocean waters; present the possibility of productive regions under Antarctic sea ice. Due to its remoteness and the presence of sea ice, these regions have not been as extensively sampled in *in situ* ecological studies or surveyed via remote sensing.

Here we examine a series of climate model estimates of light availability under Southern Ocean sea ice to understand whether the ice-covered Southern Ocean has the potential for widespread UIBs, supplemented with a map of under-ice light derived from ICESat-2 laser altimetery. We find using basic estimates for sufficient levels of photosynthetically available radiation (PAR, 400-700 nm) for positive photosynthesis of known under-ice phytoplankton species, wide areas comprising greater than 50% of the springtime Antarctic sea ice cover permit under-ice productivity. The area permitting an UIB is generally larger than the comparably well-studied Arctic Ocean, and makes up a larger proportion of the compact sea ice cover. Focusing specifically on the Ross Sea, we identify potential sampling regions for testing the hypothesis of under-ice primary production close to continuously-occupied research bases and frequently visited by research vessels in ice-free conditions.

2 Methodology

We first approximate the light field under sea ice using the ICESat-2 (IS2) laser altimeter. We utilize the L3A along-track sea ice type product (ATL07, (Kwok et al., 2019)) derived from Level 2A ATL03 photon heights (Neumann et al., 2019). Sea ice types are determined using an empirical decision tree, which identifies whether a given segment is ice or water. We consider the ratio of ice segment lengths to total segment lengths, a quantity, c^*, that is related to the sea ice concentration, c. Given the random orientation of crack and open water features relative to frequent satellite tracks, many such 1-D measurements can approximate of a 2-D field like sea ice areal concentration when sampled sufficiently. In (Horvat et al., 2020), global sea ice area from passive microwave (PM) was well-approximated by this method in regions where IS2 records at least 1000 individual segments per month, a threshold we use here. An advantage of using ICESat-2 segments instead of PM is reduced ambiguity of the concentration measurement: algorithmic differences can create significant uncertainty in local PM estimates of sea ice concentration (Notz et al., 2013).

Using the ICESat-2 concentration product, we make a crude approximation of the irradiance reaching the upper ocean, I_0,

$$I_0 = (1 - c^*)(1 - \alpha_{oc}) \tag{1}$$

where $\alpha_{oc} = 0.06$ is the open water albedo and SW is the downwelling solar irradiance at the surface. This simple model assumes no light passes through the sea ice surface, and the only light available under sea ice comes through leads. For this reason we expect the ICESat-2 derived irradiances to be conservative. For SW, we use the reanalyzed estimate of downwelling shortwave irradiance from (Tsujino et al., 2018). Available IS2 data spans the date range from October 2018-October 2020, which we use to form a climatology of I_0.

Remote sensing technologies are unable to directly measure light or chlorophyll through sea ice - and most sampling strategies have focused on sea-ice-associated algal communities in coastal regions (Smetacek et al., 1992; Arrigo & Thomas, 2004; McMinn et al., 2010; Cummings et al., 2019). We must turn to model estimates to describe the joint climatological light, sea ice, and ocean conditions underneath sea ice throughout the Southern Ocean. We use a set of current-generation coupled climate models contributing to the 6th Coupled Model Intercomparison Project (CMIP6). While observations show Antarctic sea ice has been stable or increased in extent over the satellite period (1978-present), CMIP6 models consistently simulate a declining annual-average Antarctic sea ice cover over this period (Roach et al., 2020). Thus we do not examine present-day estimates of Antarctic sea ice extent, which might incorporate biased depictions of sea ice albedo and extent, but instead postulate that light conditions under Antarctic sea ice have remained stable over the industrial period, and use data from pre-industrial control simulations (CMIP6 runs titled picontrol) used to spin up CMIP6 models. Of the entire CMIP6 model dataset, 11 simulations (see Supporting Table S1) submitted the required model output we use here.

The 11 models produce varying estimations of both climate and sea ice state, though there is high interrelation between the sea ice and light models: 9 of 11 sea ice models are branched from different versions of the Community Sea Ice Model (CICE). There are only three substantially different light models represented among the 11 models: the improved (Briegleb & Light, 2007) (B+L) δ-Eddington multiple-scattering scheme found in CICE versions 5 and above (CESM2 and NorESM2 simulations), an earlier version of the B+L scheme found in CICE version 4 (CAS), or implementations of simpler Beer-Lambert exponential attenuation of light in ice (CERFACS,MRI). We make this note only to illustrate the general interrelatedness of current-generation sea ice models, which could contribute consistent biases in Antarctic sea ice state.

For each contribution, we create a climatology of light and sea ice properties using the final 100 years of the pre-industrial spinup experiments. We define "under ice" blooms as those that occur in compact ice zones, those with a local sea ice concentration exceeding 80%. This is to differentiate blooms under sea ice from those known to occur as the ice edge retreats in the marginal ice zone (Smith & Nelson, 1986; Perrette et al., 2011). We then use two criteria for whether an area permits an UIB:

An illuminated upper ocean. Average PAR in the top 25 meters of the ocean exceeds 10 μmol photons/m^2/s.

A stable or stratifying surface mixed layer. Sea ice is not refreezing and the upper ocean is non-convecting.

For both IS-2 and CMIP6 surface irradiance (including contributions both from open water and through sea ice) fields I_0, we estimate the average PAR at a depth D as,

$$\overline{I} = \frac{I_0}{\kappa D}\left[1 - \exp(-\kappa D)\right]. \tag{2}$$

Here we assume that PAR is attenuated exponentially in water with a coefficient κ.

We assume positive photosynthesis (gains outweigh losses) occurs when the average PAR over a 25 m deep water column exceeds 10 μmol photons / m^2/s. This is approximately twice the threshold of integrated daily irradiance of 0.415 mol photons / m^2/d considered to initiate a phytoplankton bloom (Letelier et al., 2004; Boss & Behrenfeld, 2010; Oziel et al., 2019), and higher than the levels found to initiate growth (Arteaga et al., 2020; Hague & Vichi, 2021). Using $\kappa = 0.081/m$ (Matthes et al., 2019) for PAR extinction in clear waters and $D = 25$m establishes a PAR threshold value for blooms: $I_0^* \approx 23$ μmol photons /m^2/s. CMIP6 models typically store and output full-spectrum solar forcing to the upper ocean, but not PAR. We therefore convert full spectrum solar irradiance to PAR using a factor of 1.9975 μmol photons/J (Yu et al., 2015; Matthes et al., 2019).

Expected phytoplankton blooming species do not have the ability to remain in the euphotic zone if the upper ocean is unstratified or convecting. Under-ice blooms are thereby unlikely when active convection in leads drives species below the euphotic zone, such as when leads are actively refreezing with the ocean at its freezing point (Lowry et al., 2018). We therefore will only consider a region capable of permitting a bloom if the upper ocean is not convecting, as in the condition of "turbulent shutdown" invoked for mid-latitude

blooms (Taylor & Ferrari, 2011). The GCMs used here are too coarse to resolve the complex boundary layer dynamics that results from surface melting of sea ice (Holland, 2003; Horvat et al., 2016; Pellichero et al., 2017), and are not suited for determining the precise convective state of the upper ocean in the presence of sea ice. We consider the ocean appropriate for blooms if sea ice is in a state of melting at its base, which occurs for an ocean temperature above freezing and would stratify the upper ocean . Requiring simply non-zero basal melting does not restrict the location of UIBs as small monthly-averaged basal melt rates occur whenever sea ice is present. We instead set a threshold for the sea ice basal melt rate $\dot{h}$. $\dot{h}$ can be expressed as an equivalent heat flux $Q = \rho L_f \dot{h}$, where $\rho_i = 920$ kg/m^3 is the sea ice density and $L_f = 3.34 \times 10^{-5}$ J/kg the latent heat of fusion. We require Q to be greater than 5 W/m^2, which corresponds to approximately $\dot{h} = 5$ cm/month of sea ice basal melt.

3 Light availability and bloom potential under Antarctic Sea Ice

We first compare the IS2-derived surface PAR to a single model, the Community Earth System Model version 2 (CESM2, (Danabasoglu et al., 2020)), using the final 100 years of the 1200-year pre-industrial control run submitted to CMIP6 and described in (Danabasoglu et al., 2020). We choose CESM2 as its sea ice component, the Community Sea Ice Model (CICE) (Hunke et al., 2015), is the base sea ice model used for 6 of 11 models considered here. CESM2 produces an overall mean state of Antarctic sea ice that is broadly realistic compared to other CMIP6 models (Roach et al., 2020; Singh et al., 2020). Similar output from CESM2 was analysed to evaluate Arctic blooms in (Ardyna et al., 2020).

Whereas the ICESat-2 model assumes no light transmission through ice, CICE5.1 has an updated "Delta-Eddington" multiple-scattering radiative transfer parameterization within sea ice (Holland et al., 2012), which uses the thickness, surface type, and other inherent optical properties of a medium to derive its reflectivity (albedo) and transmission of solar radiation. Ice optical properties are computed semi-empirically based on physical measurements on sea ice of all ages and thicknesses (Grenfell & Maykut, 1977; Perovich, 1996); that is snow-covered, bare or ponded (Warren & Wiscombe, 1980; Light, 2004; Flanner & Zender, 2006). It also includes secondary impacts of biological material, brine, or other contaminants (Cox & Weeks, 1983; SooHoo et al., 1987). The (Briegleb & Light, 2007) δ-Eddington scheme has been extensively validated, accurately reproduc-

ing AOPs of Arctic sea ice of all of the above mentioned ice types (Briegleb & Light, 2007; Light et al., 2008), and different versions of this scheme are employed by 8 of 11 models considered below.

In Figure 1(a), we show IS-2-derived average I_0 values in Antarctica in November (darker is more PAR). A solid white line shows the outline of the compact ice zone (CIZ), defined as the region with sea ice concentration greater than 80% - where sea ice concentration is determined using the NASATEAM passive microwave product (Cavalieri et al., 1996). We also plot the 15% sea ice concentration contour, demonstrating the overall sea ice extent (SIE). Regions lying inside the SIE contour but outside the CIZ are the marginal ice zones (MIZ), which are known to be highly productive (Arrigo & Thomas, 2004). Due to the high albedo of sea ice, the MIZ experiences significantly higher PAR values than the CIZ. Figure 1(b) shows the CESM2 picontrol average I_0 values for November around Antarctica, with the CIZ/MIZ defined from the model climatology. Both IS-2 and CESM2 estimates show large regions inside the climatological compact ice zone extent with sufficiently high surface PAR. Figure 1(c) plots the fraction of all November months in the 100 CESM picontrol years where a grid cell permits an UIB. Indeed, large areas of the November Southern Ocean, in particular the Ross Sea, are covered by compact sea ice with sufficiently high solar input and oceanographic conditions, and generally lie between the coast and the marginal ice zone. Because of internal variability of the CIZ, regions outside of the climatological CIZ have non-zero UIB%.

Figure 1(c) plots the climatological seasonal cycle of total compact ice extent (red solid), sea ice extent (red dashed), and area supporting UIBs from CESM2 (blue), with an annual cycle centered on austral summer. Large regions of the Southern Ocean support UIBs from October-January, peaking in November when 6.3 million km^2 of compact ice-covered regions permit UIBs. We also indicate the area supporting UIBs from ICESat-2 (dashed green), however note that because we do not have coincident ocean and sea ice melt statistics, IS-2 estimates only indicate the presence of light in the upper ocean and may overestimate the area that permits a UIB. Up to 9.2 million km^2 of the upper ocean receives enough sunlight to permit a 25-meter bloom according to the IS-2 product.

Due to the variable CIZ extent between models, between hemispheres, and from year-to-year, an important variable is the fraction of the CIZ that leads to UIB forma-

tion in a given region. This fraction (which we define as the UIB%) is given as a solid black line (corresponding to the right axis) for the CESM2 data. Antarctic UIB% peaks in December, with 77% of the CESM2 Antarctic compact sea ice cover permitting an UIB. By point of comparison, we reproduce Figure 1(c) as Figure 1(d) for CESM2, considering the Arctic sea ice cover (note the seasonal cycle in (d) is centered on June 21). Up to 4.3 million km^2 of the pre-industrial Arctic CIZ is permissive to UIBs, repeating the finding in (Ardyna et al., 2020), that large regions of the pre-industrial Arctic also supported UIBs. The fraction of compact sea ice permitting UIBs in the Arctic peaks at 52% in July. Generally in the CESM2 picontrol simulation, we find that UIB-permitting regions are larger and take up a larger fraction of the Antarctic CIZ than of the Arctic CIZ.

Southern Ocean UIB statistics across CMIP6 models

Figure 2(a) shows the climatological seasonal cycle of UIB area for each model, similar to the blue curve shown in Figure 1(c). Each exhibits a similar seasonal cycle, with negligible UIB areas except from October to January. 10 of the 11 models (including the 4 CESM2-based models) have a maximum UIB area in November, while MRI-ESM2 has a maximum in December. In Figure 2(c), we show box plots of UIB area in the month with the climatological maximum UIB area for each model, formed from the 100 pre-industrial years in each model (colors correspond to colors of line plots in (a)). All models show the maximum Arctic UIB area in June. In all but three models (FGOALS-g3, MRI-ESM2, and NorESM2-MM) the maximum Antarctic UIB areas exceed the maximum values in the Arctic.

In Figure 2(b,d), we repeat Figure 2(a,c) for the Antarctic UIB%. The seasonal cycle of Antarctic UIB% is again broadly similar, with most models peaking in December as the CIZ reduces in extent and light increases. All 11 models have higher UIB% in the Antarctic (from 32% to 78%) compared to the Arctic (from 31% to 59%). Thus, the reason the three models in Figure 2(c) have larger maximum UIB areas in the Arctic than the Antarctic can be explained by these three models having the largest June CIZ extents by a wide margin. For example, the NorESM2-MM model produced both the highest June Arctic CIZ extent and lowest November Antarctic CIZ extent.

4 The Ross Sea

We now turn to an examination of the Ross Sea region, an area that is seasonally ice-free and has been the site of significant research interest into ice-associated ecological activity. The Ross Sea ice is located near to the most active and highly-populated scientific research stations and is frequently visited by oceanographic cruises, mainly in ice-free months. To define the "Ross Sea region", we roughly follow the convention established by the NIWA Ross Sea Trophic Model (Pinkerton et al., 2010), taking the ocean region south of 69°S and between 160°W and 170°E longitude. Because of grid variations, the area of this region can vary between models, but its surface area is approximately 1.5 million km^2.

In Figure 3, we show the number of years out of 100 where an UIB is permitted for this set of models during the month with the maximum Ross Sea UIB extent, which is November in 7 out of 11 models, and December for 4 out of 11 (CAS-ESM2,CNRM-CM6,CNRM-ESM2, and MRI-ESM2). Areas where UIB formation is possible vary between models, though all models show a high UIB likelihood in the coastal region near Cape Adare in the Western Ross Sea, which has compact sea ice into summer and is identified by a blue square.

Figure 4 shows the seasonal cycle of Ross Sea UIB area (a), Ross Sea UIB% (b), and the box plots of both for each model in the month of maximum UIB area (c,d). Generally up to 0.5 million km^2 of the Ross Sea are expected to permit UIBs. However, the geographic borders of UIB-permitting areas vary by model (see Fig. 3), and there is considerable interannual variability (whiskers). For nearly all models (excluding FGOALS-g3, which also has the smallest CIZ in the Ross area), on average more than half of the Ross Sea CIZ permits UIBs in the peak months of November or December.

5 Discussion

We demonstrated that observed and modeled sea ice, light, and oceanographic conditions across the compact-ice-covered Southern Ocean in general, and in the Ross Sea in particular, may permit widespread under-ice primary production. The climate models considered here have inter-related sea ice and light schemes, and provide estimates of the light conditions in the Southern Ocean, but may not be accurate if systematic biases in modeled Southern Ocean climate or sea ice exist. Still, when compared against

an estimate of upper ocean PAR derived from ICESat-2 data, models produce similar PAR estimates, and may underestimate the area permitting UIBs.

The method for inferring the presence of UIBs here is based on a simple set of diagnostic criteria, not detailed biogeochemical modeling, and uses bulk estimates for light transmission and photosynthesis, and a sea-ice melt-based estimate of when the upper ocean is stratifiying. Whether more sophisticated ocean ecological parameterizations will be able to address the prevalence of Antarctic UIBs is unclear. Such models depend on versions of the very same coupled ice-ocean models used here, and are tuned on the basis of observations - which by necessity come from outside of sea ice-covered regions. For example, a recent intercomparison of biogeochemical models suggested that under-ice primary production *decreased* in the Arctic over the period from 1980-2009 (Jin et al., 2016), despite increased solar forcing to under-ice regions. There is substantial evidence that productivity has increased: greater productivity of sea ice-algal communities (Tedesco et al., 2019), enhanced production of atmospheric iodine in under-ice ecosystems (Cuevas et al., 2018), and frequent observations of summer Arctic UIBs (Ardyna et al., 2020). Without complementary *in situ* observations, more complex models may not necessarily be a reliable gauge of the existence of Antarctic UIBs. Indeed, model results shown in this study qualitatively agree with the recent BGC-ARGO studies of (Arteaga et al., 2020; Hague & Vichi, 2021), who found phytoplankton growth likely precedes the retreat of seasonal sea ice across the Southern Ocean.

This work suggests that there is an unexplored and unobserved ecosystem under sea ice, with 3-6 million square kilometers of the ice-covered Southern Ocean potentially permitting primary production before the seasonal retreat of the sea ice edge. The hypothesis of a highly productive Southern Ocean under sea ice during the Antarctic summer ought to be tested through field sampling, and we paid special attention to the more-frequently visited Ross Sea region. Field sampling will be necessary to validate these observations, including detailed measurements of physical and biogeochemical variables to identify the blooming species in this region and determine whether bloom dynamics are similar to the Arctic (Chase et al., 2020). Sampling during the sea ice-covered season will be challenging, but Remotely Operated Vehicles (ROV) and autonomous profiling floats (Arteaga et al., 2020; Hague & Vichi, 2021) are increasingly being deployed in ice-infested conditions in Antarctica (Moreau et al., 2020) complementary to ship-based sampling. Since timing is one of the main constraints to ensure under ice bloom observations,

a long seasonal sampling beginning in austral spring, similar to the methodologies used in the Arctic, would increase the likelihood of observing the development of an under-ice bloom. Such direct measurements will help determine the dynamics of under-ice bloom development. Additionally, long-term monitoring work can fill in observational gaps, covering the entire seasonal cycle. We identified a region in the western Ross Sea, roughly at the position of Cape Adare in the Ross Dependency, which has the requisite conditions for blooming in all models and may be more accessible in late spring to ascertain whether these blooms occur.

In addition to *in situ* measurements, we note the promise of satellite laser altimetry, specifically ICESat-2. We used a simple method for inferring upper-ocean PAR under sea ice, which can potentially be greatly improved, by simultaneously considering sea ice thickness and snow depth profiles which can permit more sophisticated modeling of the light field in and under ice (Kwok & Markus, 2018; Kwok et al., 2020). ICESat-2 also has shown promise for directly retrieving the signature of phytoplankton biomass in ice-free regions (Lu et al., 2020). Because of the high along-track resolution and noted accuracy of ICESat-2 for delineating leads and cracks from sea ice, it may be possible to extend these open water measurements underneath sea ice and directly investigate the question of under-ice productivity at the global scale to compare with climate models.

Acknowledgments

CH was supported by NASA grant 80NSSC20K0959. KB was supported by NASA grant 80NSSC20K0970.

Data Availability

ICESat-2 data are available through the National Snow and Ice Data Center (NSIDC). The sea ice type product is found online at https://nsidc.org/data/ATL07/versions/3. JRA55-do and CMIP6 data used in this study are available at the Earth System Federated Grid at `https://esgf-node.llnl.gov/projects/input4MIPs/` and `https://esgf-node.llnl.gov/proj` respectively. Code for processing data and producing Antarctic under-ice light fields and UIB-permitting criteria will be publicly developed on github at https://github.com/chhorvat/Antarctic-Light/ with releases archived in the Zenodo repository (Horvat et al., 2021).

References

Ardyna, M., Mundy, C. J., Mayot, N., Matthes, L. C., Oziel, L., Horvat, C., ... Arrigo, K. R. (2020, nov). Under-Ice Phytoplankton Blooms: Shedding Light on the "Invisible" Part of Arctic Primary Production. *Frontiers in Marine Science*, *7*(November), 1–25. Retrieved from https://www.frontiersin.org/articles/10.3389/fmars.2020.608032/full doi: 10.3389/fmars.2020.608032

Arndt, S., Meiners, K. M., Ricker, R., Krumpen, T., Katlein, C., & Nicolaus, M. (2017, mar). Influence of snow depth and surface flooding on light transmission through Antarctic pack ice. *Journal of Geophysical Research: Oceans*, *122*(3), 2108–2119. Retrieved from http://www.nature.com/articles/175238c0http://doi.wiley.com/10.1002/2016JC012325 doi: 10.1002/2016JC012325

Arrigo, K. R. (1999, jan). Phytoplankton Community Structure and the Drawdown of Nutrients and CO2 in the Southern Ocean. *Science*, *283*(5400), 365–367. Retrieved from https://www.sciencemag.org/lookup/doi/10.1126/science.283.5400.365 doi: 10.1126/science.283.5400.365

Arrigo, K. R., Perovich, D. K., Pickart, R. S., Brown, Z. W., van Dijken, G. L., Lowry, K. E., ... Swift, J. H. (2012, jun). Massive Phytoplankton Blooms Under Arctic Sea Ice. *Science*, *336*(6087), 1408. Retrieved from http://www.sciencemag.org/cgi/doi/10.1126/science.1215065 doi: 10.1126/science.1215065

Arrigo, K. R., & Thomas, D. N. (2004). Large scale importance of sea ice biology in the Southern Ocean. *Antarctic Science*, *16*(4), 471–486. doi: 10.1017/S0954102004002263

Arrigo, K. R., van Dijken, G. L., Alderkamp, A., Erickson, Z. K., Lewis, K. M., Lowry, K. E., ... van de Poll, W. (2017, dec). Early Spring Phytoplankton Dynamics in the Western Antarctic Peninsula. *Journal of Geophysical Research: Oceans*, *122*(12), 9350–9369. Retrieved from https://onlinelibrary.wiley.com/doi/abs/10.1002/2017JC013281 doi: 10.1002/2017JC013281

Arteaga, L. A., Boss, E., Behrenfeld, M. J., Westberry, T. K., & Sarmiento, J. L. (2020). Seasonal modulation of phytoplankton biomass in the Southern

Ocean. *Nature Communications*, *11*(1). Retrieved from http://dx.doi.org/10.1038/s41467-020-19157-2 doi: 10.1038/s41467-020-19157-2

Assmy, P., Fernández-Méndez, M., Duarte, P., Meyer, A., Randelhoff, A., Mundy, C. J., ... Granskog, M. A. (2017, dec). Leads in Arctic pack ice enable early phytoplankton blooms below snow-covered sea ice. *Scientific Reports*, *7*(1), 40850. Retrieved from http://www.nature.com/articles/srep40850 doi: 10.1038/srep40850

Biggs, T. E. G., Alvarez-Fernandez, S., Evans, C., Mojica, K. D. A., Rozema, P. D., Venables, H. J., ... Brussaard, C. P. D. (2019, nov). Antarctic phytoplankton community composition and size structure: importance of ice type and temperature as regulatory factors. *Polar Biology*, *42*(11), 1997–2015. Retrieved from http://link.springer.com/10.1007/s00300-019-02576-3 doi: 10.1007/s00300-019-02576-3

Boss, E., & Behrenfeld, M. (2010, sep). In situ evaluation of the initiation of the North Atlantic phytoplankton bloom. *Geophysical Research Letters*, *37*(18), 1–5. doi: 10.1029/2010GL044174

Brandt, R. E., Warren, S. G., Worby, A. P., & Grenfell, T. C. (2005, sep). Surface Albedo of the Antarctic Sea Ice Zone. *Journal of Climate*, *18*(17), 3606–3622. Retrieved from https://journals.ametsoc.org/jcli/article/18/17/3606/30648/Surface-Albedo-of-the-Antarctic-Sea-Ice-Zone doi: 10.1175/JCLI3489.1

Briegleb, B. P., & Light, B. (2007). *A Delta-Eddington multiple scattering parameterization for solar radiation in the sea ice component of the Community Climate System Model* (Vol. NCAR/TN-47; Tech. Rep. No. February). National Center for Atmospheric Research. Technical Note TN-472STR, National Center for Atmospheric Research, Boulder, CO, United States. doi: 10.5065/D6B27S71

Cavalieri, D. J., Parkinson, C. L., Gloerson, P., & Zwally, H. J. (1996). *Sea Ice Concentrations from Nimbus-7 SMMR and DMSP SSM/I-SSMIS Passive Microwave Data.* NASA National Snow and Ice Data Center Distributed Active Archive Center. doi: 10.5067/8GQ8LZQVL0VL

Chase, A. P., Kramer, S. J., Haëntjens, N., Boss, E. S., Karp-Boss, L., Edmondson, M., & Graff, J. R. (2020). Evaluation of diagnostic pigments to estimate

phytoplankton size classes. *Limnology and Oceanography: Methods*. doi: 10.1002/lom3.10385

Comiso, J. C., McClain, C. R., Sullivan, C. W., Ryan, J. P., & Leonard, C. L. (1993, feb). Coastal zone color scanner pigment concentrations in the Southern Ocean and relationships to geophysical surface features. *Journal of Geophysical Research: Oceans*, *98*(C2), 2419–2451. Retrieved from `http://doi.wiley.com/10.1029/92JC02505` doi: 10.1029/92JC02505

Cox, G. F. N., & Weeks, W. F. (1983, jan). Equations for Determining the Gas and Brine Volumes in Sea-Ice Samples. *Journal of Glaciology*, *29*(102), 306–316. Retrieved from `https://www.cambridge.org/core/product/identifier/S0022143000008364/type/journal{\_}article` doi: 10.1017/S0022143000008364

Cuevas, C. A., Maffezzoli, N., Corella, J. P., Spolaor, A., Vallelonga, P., Kjær, H. A., ... Saiz-Lopez, A. (2018). Rapid increase in atmospheric iodine levels in the North Atlantic since the mid-20th century. *Nature Communications*, *9*(1), 1452. doi: 10.1038/s41467-018-03756-1

Cummings, V. J., Barr, N. G., Budd, R. G., Marriott, P. M., Safi, K. A., & Lohrer, A. M. (2019, dec). In situ response of Antarctic under-ice primary producers to experimentally altered pH. *Scientific Reports*, *9*(1), 6069. Retrieved from `http://dx.doi.org/10.1038/s41598-019-42329-0http://www.nature.com/articles/s41598-019-42329-0` doi: 10.1038/s41598-019-42329-0

Danabasoglu, G., Lamarque, J. F., Bacmeister, J., Bailey, D. A., DuVivier, A. K., Edwards, J., ... Strand, W. G. (2020). The Community Earth System Model Version 2 (CESM2). *Journal of Advances in Modeling Earth Systems*, *12*(2), 1–35. doi: 10.1029/2019MS001916

Davidson, A. T., Scott, F. J., Nash, G. V., Wright, S. W., & Raymond, B. (2010, may). Physical and biological control of protistan community composition, distribution and abundance in the seasonal ice zone of the Southern Ocean between 30 and 80E. *Deep Sea Research Part II: Topical Studies in Oceanography*, *57*(9-10), 828–848. Retrieved from `https://linkinghub.elsevier.com/retrieve/pii/S0967064509003920` doi: 10.1016/j.dsr2.2009.02.011

Deppeler, S. L., & Davidson, A. T. (2017, feb). Southern Ocean Phytoplankton in a Changing Climate. *Frontiers in Marine Science*, *4*(FEB). Retrieved from

http://journal.frontiersin.org/article/10.3389/fmars.2017.00040/full doi: 10.3389/fmars.2017.00040

Flanner, M. G., & Zender, C. S. (2006). Linking snowpack microphysics and albedo evolution. *Journal of Geophysical Research*, *111*(D12), D12208. Retrieved from http://doi.wiley.com/10.1029/2005JD006834 doi: 10.1029/2005JD006834

Gelaro, R., McCarty, W., Suárez, M. J., Todling, R., Molod, A., Takacs, L., ... Zhao, B. (2017, jul). The Modern-Era Retrospective Analysis for Research and Applications, Version 2 (MERRA-2). *Journal of Climate*, *30*(14), 5419–5454. Retrieved from https://journals.ametsoc.org/doi/10.1175/JCLI-D-16-0758.1 doi: 10.1175/JCLI-D-16-0758.1

Grenfell, C., & Maykut, G. A. (1977). The optical properties of ice and snow in the Arctic Basin. *J. Glaciol.*, *18*(80), 445–463. doi: 10.1017/S0022143000021122

Hague, M., & Vichi, M. (2021, jan). Southern Ocean Biogeochemical Argo detect under-ice phytoplankton growth before sea ice retreat. *Biogeosciences*, *18*(1), 25–38. Retrieved from https://bg.copernicus.org/articles/18/25/2021/ doi: 10.5194/bg-18-25-2021

Holland, M. M. (2003). An improved single-column model representation of ocean mixing associated with summertime leads: Results from a SHEBA case study. *Journal of Geophysical Research*, *108*(C4), 3107. Retrieved from http://doi.wiley.com/10.1029/2002JC001557 doi: 10.1029/2002JC001557

Holland, M. M., Bailey, D. A., Briegleb, B. P., Light, B., & Hunke, E. (2012). Improved sea ice shortwave radiation physics in CCSM4: The impact of melt ponds and aerosols on Arctic sea ice. *Journal of Climate*, *25*(5), 1413–1430. doi: 10.1175/JCLI-D-11-00078.1

Horvat, C., Blanchard-Wrigglesworth, E., & Petty, A. (2020, apr). Observing waves in sea ice with ICESat-2. *Geophysical Research Letters*. Retrieved from https://onlinelibrary.wiley.com/doi/abs/10.1029/2020GL087629 doi: 10.1029/2020GL087629

Horvat, C., Seabrook, S., Cristi, A., Matthes, L., & Bisson, K. (2021). *Code for: The Case for Phytoplankton Blooms Under Antarctic Sea Ice.* doi: 10.5281/zenodo.4579199

Horvat, C., Tziperman, E., & Campin, J.-M. (2016, aug). Interaction of sea ice floe

size, ocean eddies, and sea ice melting. *Geophysical Research Letters*, *43*(15), 8083–8090. Retrieved from http://doi.wiley.com/10.1002/2016GL069742 doi: 10.1002/2016GL069742

Hunke, E. C., Lipscomb, W. H., Turner, A. K., Jeffery, N., & Elliott, S. (2015). *CICE : the Los Alamos Sea Ice Model Documentation and Software User's Manual Version 5.1 LA-CC-06-012* (Tech. Rep.). Los Alamos National Laboratory. Retrieved from http://oceans11.lanl.gov/trac/CICE

Jin, M., Popova, E. E., Zhang, J., Ji, R., Pendleton, D., Varpe, Ø., ... Lee, Y. J. (2016, jan). Ecosystem model intercomparison of under-ice and total primary production in the Arctic Ocean. *Journal of Geophysical Research: Oceans*, *121*(1), 934–948. doi: 10.1002/2015JC011183

Kwok, R., Cunningham, G., Markus, T., Hancock, D., Morison, J., Palm, S. P., ... Team, t. I.-. S. (2019). *ATLAS/ICESat-2 L3A Sea Ice Height, Version 1. Boulder, Colorado USA.* (Tech. Rep. No. May). Boulder, Colorado USA: NSIDC. doi: https://doi.org/10.5067/ATLAS/ATL07.001

Kwok, R., Kacimi, S., Webster, M., Kurtz, N., & Petty, A. (2020, mar). Arctic Snow Depth and Sea Ice Thickness From ICESat-2 and CryoSat-2 Freeboards: A First Examination. *Journal of Geophysical Research: Oceans*, *125*(3). Retrieved from https://onlinelibrary.wiley.com/doi/abs/10.1029/2019JC016008 doi: 10.1029/2019JC016008

Kwok, R., & Markus, T. (2018, sep). Potential basin-scale estimates of Arctic snow depth with sea ice freeboards from CryoSat-2 and ICESat-2: An exploratory analysis. *Advances in Space Research*, *62*(6), 1243–1250. Retrieved from https://linkinghub.elsevier.com/retrieve/pii/S0273117717306403 doi: 10.1016/j.asr.2017.09.007

Letelier, R. M., Karl, D. M., Abbott, M. R., & Bidigare, R. R. (2004). Light driven seasonal patterns of chlorophyll and nitrate in the lower euphotic zone of the North Pacific Subtropical Gyre. *Limnology and Oceanography*, *49*(2), 508–519. doi: 10.4319/lo.2004.49.2.0508

Light, B. (2004). A temperature-dependent, structural-optical model of first-year sea ice. *Journal of Geophysical Research*, *109*(C6), C06013. Retrieved from http://doi.wiley.com/10.1029/2003JC002164 doi: 10.1029/2003JC002164

Light, B., Grenfell, T. C., & Perovich, D. K. (2008, mar). Transmission and absorption of solar radiation by Arctic sea ice during the melt season. *Journal of Geophysical Research: Oceans*, *113*(3), C03023. Retrieved from http://doi.wiley.com/10.1029/2006JC003977 doi: 10.1029/2006JC003977

Lowry, K. E., Pickart, R. S., Selz, V., Mills, M. M., Pacini, A., Lewis, K. M., ... Arrigo, K. R. (2018, jan). Under-Ice Phytoplankton Blooms Inhibited by Spring Convective Mixing in Refreezing Leads. *Journal of Geophysical Research: Oceans*, *123*(1), 90–109. Retrieved from http://doi.wiley.com/10.1002/2016JC012575 doi: 10.1002/2016JC012575

Lu, X., Hu, Y., Yang, Y., Bontempi, P., Omar, A., & Baize, R. (2020). Antarctic spring ice-edge blooms observed from space by ICESat-2. *Remote Sensing of Environment*, *245*(November 2019), 111827. Retrieved from https://doi.org/10.1016/j.rse.2020.111827 doi: 10.1016/j.rse.2020.111827

Martin, J. H., Fitzwater, S. E., & Gordon, R. M. (1990, mar). Iron deficiency limits phytoplankton growth in Antarctic waters. *Global Biogeochemical Cycles*, *4*(1), 5–12. Retrieved from http://doi.wiley.com/10.1029/GB004i001p00005 doi: 10.1029/GB004i001p00005

Matthes, L. C., Ehn, J. K., Girard, S. L., Pogorzelec, N. M., Babin, M., & Mundy, C. J. (2019). Average cosine coefficient and spectral distribution of the light field under sea ice: Implications for primary production. *Elementa*, *7*(1). doi: 10.1525/elementa.363

McMinn, A., Martin, A., & Ryan, K. (2010, nov). Phytoplankton and sea ice algal biomass and physiology during the transition between winter and spring (McMurdo Sound, Antarctica). *Polar Biology*, *33*(11), 1547–1556. Retrieved from http://www.nature.com/articles/175238c0http://doi.wiley.com/10.1002/2016JC012325http://link.springer.com/10.1007/s00300-010-0844-6 doi: 10.1007/s00300-010-0844-6

Montes-Hugo, M., Vernet, M., Martinson, D., Smith, R., & Iannuzzi, R. (2008, sep). Variability on phytoplankton size structure in the western Antarctic Peninsula (1997–2006). *Deep Sea Research Part II: Topical Studies in Oceanography*, *55*(18-19), 2106–2117. Retrieved from https://linkinghub.elsevier.com/retrieve/pii/S0967064508001604 doi: 10.1016/j.dsr2.2008.04.036

Moreau, S., Boyd, P. W., & Strutton, P. G. (2020). Remote assessment of the fate

of phytoplankton in the Southern Ocean sea-ice zone. *Nature Communications*. doi: 10.1038/s41467-020-16931-0

Neumann, T. A., Martino, A. J., Markus, T., Bae, S., Bock, M. R., Brenner, A. C., ... Thomas, T. C. (2019, nov). The Ice, Cloud, and Land Elevation Satellite – 2 mission: A global geolocated photon product derived from the Advanced Topographic Laser Altimeter System. *Remote Sensing of Environment*, *233*, 111325. Retrieved from `https://linkinghub.elsevier.com/retrieve/pii/S003442571930344X` doi: 10.1016/j.rse.2019.111325

Notz, D., Haumann, F. A., Haak, H., Jungclaus, J. H., & Marotzke, J. (2013, jun). Arctic sea-ice evolution as modeled by Max Planck Institute for Meteorology's Earth system model. *Journal of Advances in Modeling Earth Systems*, *5*(2), 173–194. Retrieved from `http://dx.doi.org/10.1002/jame.20016http://doi.wiley.com/10.1002/jame.20016` doi: 10.1002/jame.20016

Oziel, L., Massicotte, P., Randelhoff, A., Ferland, J., Vladoiu, A., Lacour, L., ... Babin, M. (2019, jan). Environmental factors influencing the seasonal dynamics of spring algal blooms in and beneath sea ice in western Baffin Bay. *Elementa: Science of the Anthropocene*, *7*(1), 34. Retrieved from `https://online.ucpress.edu/elementa/article/doi/10.1525/elementa.372/112501/Environmental-factors-influencing-the-seasonal` doi: 10.1525/elementa.372

Pellichero, V., Sallée, J.-B., Schmidtko, S., Roquet, F., & Charrassin, J.-B. (2017, feb). The ocean mixed layer under Southern Ocean sea-ice: Seasonal cycle and forcing. *Journal of Geophysical Research: Oceans*, *122*(2), 1608–1633. Retrieved from `http://doi.wiley.com/10.1002/2016JC011970` doi: 10.1002/2016JC011970

Perovich, D. K. (1996). The Optical Properties of Sea Ice. *CRREL Monograph*, *96-1*(May), 25.

Perrette, M., Yool, A., Quartly, G. D., & Popova, E. E. (2011, feb). Near-ubiquity of ice-edge blooms in the Arctic. *Biogeosciences*, *8*(2), 515–524. doi: 10.5194/bg-8-515-2011

Pinkerton, M. H., Bradford-Grieve, J. M., & Hanchet, S. M. (2010). A balanced model of the food web of the Ross Sea, Antarctica. *CCAMLR Science*, *17*, 1–31.

Porter, D. F., Springer, S. R., Padman, L., Fricker, H. A., Tinto, K. J., Riser, S. C., & Bell, R. E. (2019). Evolution of the Seasonal Surface Mixed Layer of the Ross Sea, Antarctica, Observed With Autonomous Profiling Floats. *Journal of Geophysical Research: Oceans*, *124*(7), 4934–4953. doi: 10.1029/2018JC014683

Roach, L. A., Doerr, J., Holmes, C. R., Massonnet, F., Blockley, E. W., Notz, D., ... Bitz, C. M. (2020). Antarctic Sea Ice Area in CMIP6. *Geophysical Research Letters*, 1–24. doi: 10.1029/2019gl086729

Singh, H. K. A., Landrum, L., Holland, M. M., Bailey, D. A., & DuVivier, A. K. (2020). An Overview of Antarctic Sea Ice in the Community Earth System Model version 2, Part I: Analysis of the Seasonal Cycle in the Context of Sea Ice Thermodynamics and Coupled Atmosphere-Ocean-Ice Processes. *Journal of Advances in Modeling Earth Systems*. doi: 10.1029/2020ms002143

Smetacek, V., Scharek, R., Gordon, L. I., Eicken, H., Fahrbach, E., Rohardt, G., & Moore, S. (1992, feb). Early spring phytoplankton blooms in ice platelet layers of the southern Weddell Sea, Antarctica. *Deep Sea Research Part A. Oceanographic Research Papers*, *39*(2), 153–168. Retrieved from `https://linkinghub.elsevier.com/retrieve/pii/019801499290102Y` doi: 10.1016/0198-0149(92)90102-Y

Smith, W. O., & Nelson, D. M. (1986, apr). Importance of Ice Edge Phytoplankton Production in the Southern Ocean. *BioScience*, *36*(4), 251–257. Retrieved from `https://academic.oup.com/bioscience/article-lookup/doi/10.2307/1310215` doi: 10.2307/1310215

SooHoo, J., Palmisano, A., Kottmeier, S., Lizotte, M., SooHoo, S., & Sullivan, C. (1987). Spectral light absorption and quantum yield of photosynthesis in sea ice microalgae and a bloom of Phaeocystis pouchetii from McMurdo Sound, Antarctica. *Marine Ecology Progress Series*, *39*(December 1984), 175–189. Retrieved from `http://www.int-res.com/articles/meps/39/m039p175.pdf` doi: 10.3354/meps039175

Taylor, J. R., & Ferrari, R. (2011). Shutdown of turbulent convection as a new criterion for the onset of spring phytoplankton blooms. *Limnology and Oceanography*, *56*(6), 2293–2307. doi: 10.4319/lo.2011.56.6.2293

Tedesco, L., Vichi, M., & Scoccimarro, E. (2019, may). Sea-ice algal phenology in a

warmer Arctic. *Science Advances*, *5*(5), eaav4830. Retrieved from https://advances.sciencemag.org/lookup/doi/10.1126/sciadv.aav4830 doi: 10.1126/sciadv.aav4830

Tsujino, H., Urakawa, S., Nakano, H., Small, R. J., Kim, W. M., Yeager, S. G., ... Yamazaki, D. (2018, oct). JRA-55 based surface dataset for driving ocean–sea-ice models (JRA55-do). *Ocean Modelling*, *130*(July), 79–139. Retrieved from https://linkinghub.elsevier.com/retrieve/pii/S146350031830235X doi: 10.1016/j.ocemod.2018.07.002

van Oijen, T. (2004, apr). Light rather than iron controls photosynthate production and allocation in Southern Ocean phytoplankton populations during austral autumn. *Journal of Plankton Research*, *26*(8), 885–900. Retrieved from https://academic.oup.com/plankt/article-lookup/doi/10.1093/plankt/fbh088 doi: 10.1093/plankt/fbh088

Warren, S. G., & Wiscombe, W. J. (1980, dec). A Model for the Spectral Albedo of Snow. II: Snow Containing Atmospheric Aerosols. *Journal of the Atmospheric Sciences*, *37*(12), 2734–2745. Retrieved from http://journals.ametsoc.org/doi/abs/10.1175/1520-0469{\%}281980{\%}29037{\%}3C2734{\%}3AAMFTSA{\%}3E2.0.CO{\%}3B2 doi: 10.1175/1520-0469(1980)037⟨2734:AMFTSA⟩2.0.CO;2

Yu, X., Wu, Z., Jiang, W., & Guo, X. (2015, jan). Predicting daily photosynthetically active radiation from global solar radiation in the Contiguous United States. *Energy Conversion and Management*, *89*, 71–82. Retrieved from https://linkinghub.elsevier.com/retrieve/pii/S0196890414008395 doi: 10.1016/j.enconman.2014.09.038

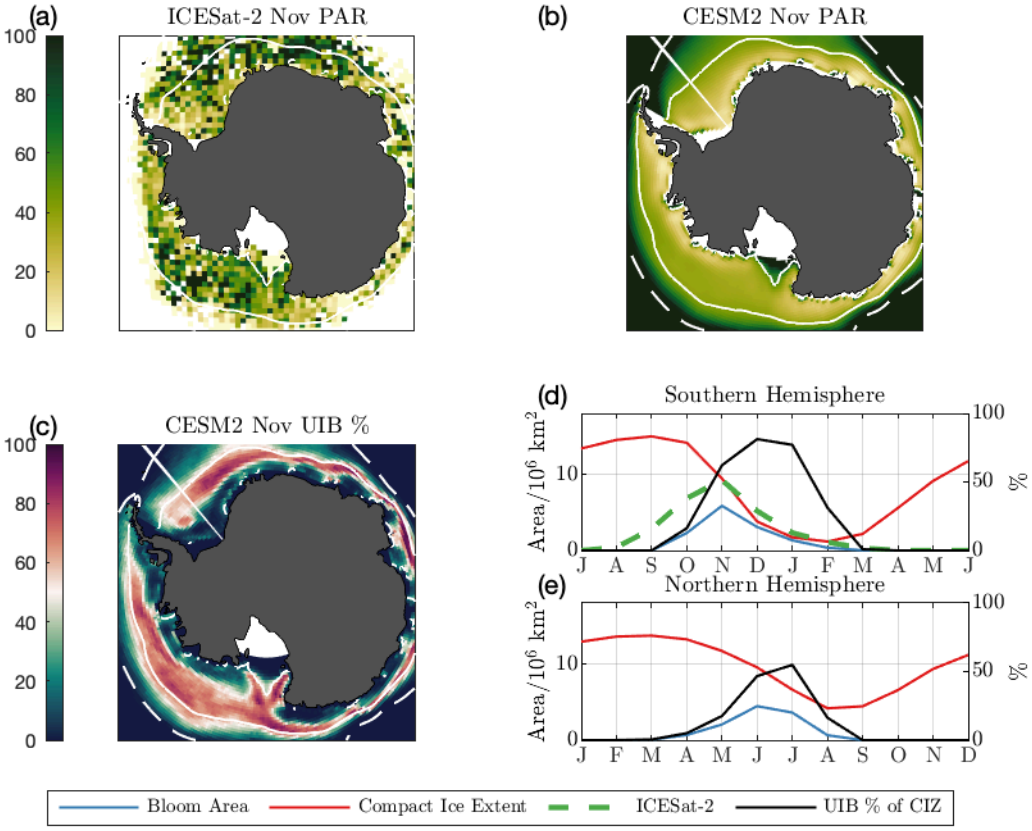

Figure 1. Light field and Bloom potential under Southern Ocean Sea Ice from ICESat-2 and the CESM2 PIControl Simulation. (a) 2018-2020 photosynthetically available radiation (PAR, units μmol/m^2/s) to the upper ocean in November from ICESat-2. (b) CESM2 climatological PAR from pre-industrial simulation. Solid white lines in (a-b) are CESM2 climatological compact ice extent (concentration above 80%). Dashed white lines are CESM2 climatological sea ice extent (concentration above 15%). (c) Percentage of CESM2 pre-industrial years where a bloom up to 25 meters deep would be permitted given the PAR reaching the upper ocean for compact ice zones. (d,left axis) Seasonal cycle of CESM2 (red) compact ice extent and (blue) compact ice areas permitting a 25 meter bloom for the Southern Hemisphere. Dashed green line is estimate of bloom-permitting regions from ICESat-2. (d,right axis) Percentage of compact ice regions where a 25 meter bloom is permitted. (e) As in (d), but for the Northern Hemisphere. Note that (d) and (e) have shifted x axes.

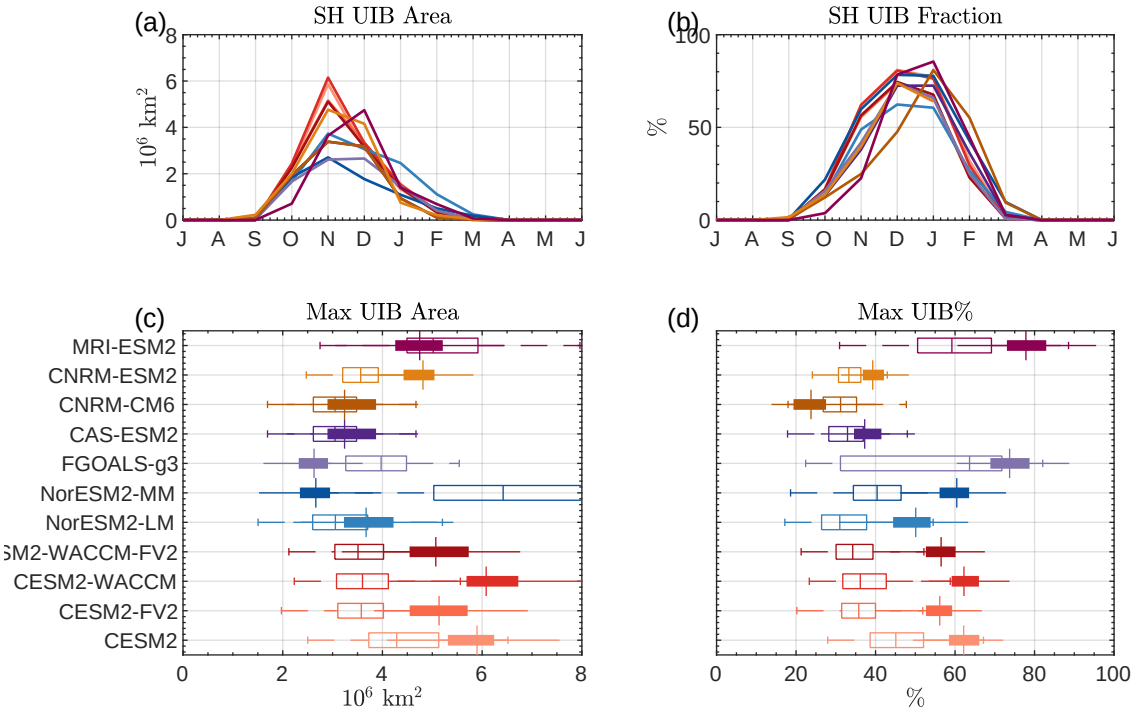

Figure 2. Statistics of Bloom-Permitting Area for all CMIP6 models examined here. (a) Total UIB-permitting area in the Southern Hemisphere. (b) Fraction of compact ice zone for each model. (c) Box plots of the maximum area permitting UIBs in (filled) the Southern Hemisphere or (empty) the Northern Hemisphere. (d) UIB fraction at the month of maximum UIB area. Colors of lines in (a,b) correspond to boxes in (c,d)

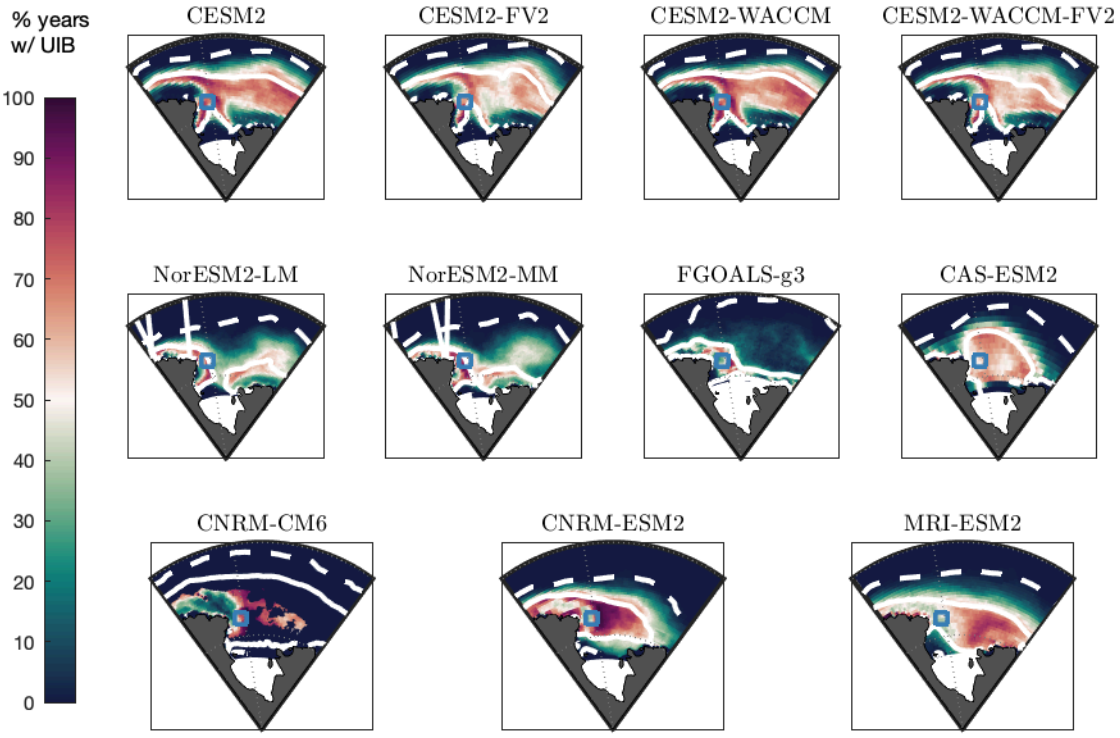

Figure 3. Percentage of preindustrial years permitting a UIB in the Ross Sea for each model in the month of maximum UIB area. Solid line is compact sea ice margin. Dashed line is marginal ice zone. Blue square is location of interest at 72°S,178^{E}.

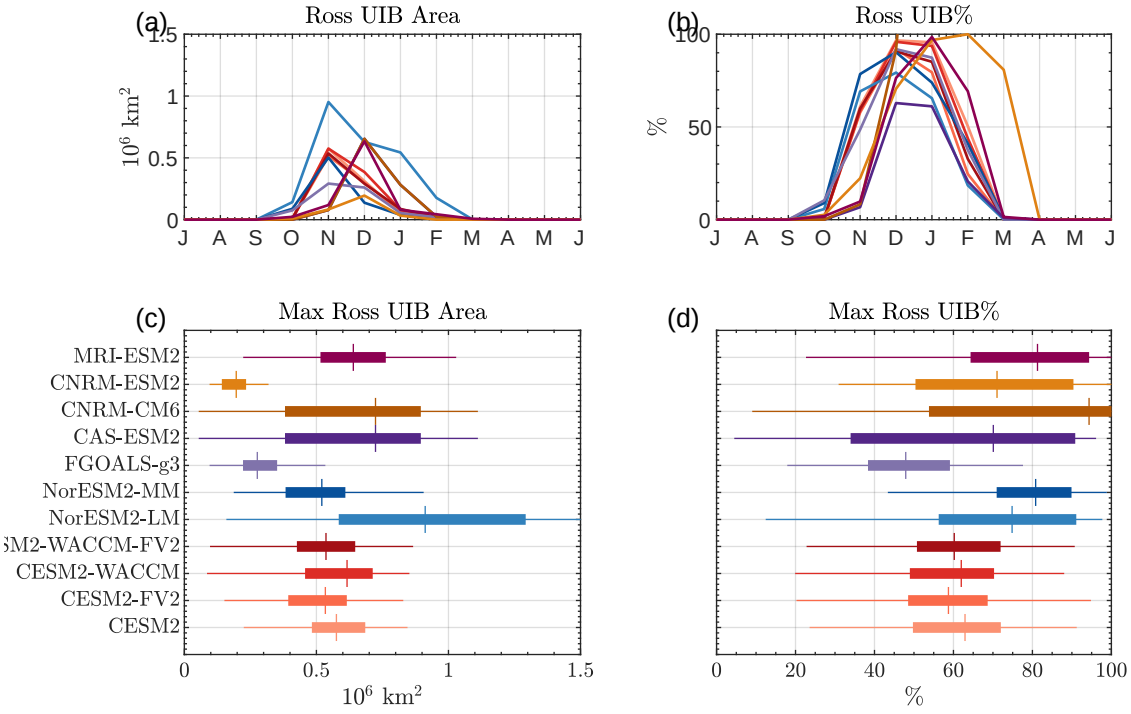

Figure 4. Climatological area of Ross Sea permitting UIBs and (b) Percentage of compact ice areas permitting blooms for each model (Ross Sea UIB%). (c) Box plot of (a) in month of maximum UIB area. (d) Box plot of (b) month of maximum UIB area. Colors of lines in (a,b) correspond to boxes in (c,d)